Chinese Journal of
POLYMER SCIENCE

RESEARCH ARTICLE

https://doi.org/10.1007/s10118-026-3597-6
Chinese J. Polym. Sci.

Water Swelling-induced Stiffness Enhancement of Polymer Hydrogels

Yi Yu[a,b], Wei Zhou[a,b], Tao Chen[a,b*], and Wei Lu[a,b*]

[a] *State Key Laboratory of Advanced Marine Materials, Ningbo Institute of Materials Technology and Engineering, Chinese Academy of Sciences, Ningbo 315201, China*
[b] *School of Chemical Sciences, University of Chinese Academy of Sciences, Beijing 100049, China*

Electronic Supplementary Information

Abstract Polymer hydrogels with variable stiffness demonstrate immense practical application value, particularly when utilizing water as a trigger medium, which significantly expands their prospects in soft robotics, bioelectronics, and artificial muscles. However, existing water-induced stiffening hydrogel rely on ionic liquids and inorganic salts, posing leakage risks during prolonged use. Here, we proposed a strategy for mechanically strengthening hydrogel through water-induced phase separation. By designing a polymer matrix featuring hydrophilic oligomeric ethylene glycol methacrylate (OEGMA) and hydrophobic methyl methacrylate (MMA) moieties, this poly[methyl methacrylate-*co*-poly(ethylene glycol) methacrylate] [P(MMA_x-*co*-$OEGMA_y$)] hydrogel exhibited reversible stiffness switching across four orders of magnitude (from 1.88×10^{-2} MPa to 201.63 MPa) upon water stimulation. This abrupt stiffness enhancement stemmed from strong hydrogen bonding between water molecules and hydrophilic OEGMA segments, facilitating spontaneous aggregation and phase separation of hydrophobic MMA segments. The resulting hydrophobic MMA domains formed dynamic physical crosslinking points, thereby enhancing the hydrogel's stiffness. Furthermore, the hydrogel exhibited a time-dependent, multi-stage stiffness enhancement during water swelling. As proof of concept, it was employed as a shape-memory component to explore its application in the controllable programming of multi-stage complex shapes, offering novel design insights for developing environmentally friendly, high-mechanical-performance smart hydrogel materials.

Keywords Polymer hydrogel; Water-induced phase separation; Stiffness enhancement; Hydrogen bonding; Shape memory

Citation: Yu, Y.; Zhou, W.; Chen, T.; Lu, W. Water swelling-induced stiffness enhancement of polymer hydrogels. *Chinese J. Polym. Sci.* https://doi.org/10.1007/s10118-026-3597-6

INTRODUCTION

Natural organisms are inherently capable of rapidly and reversibly adjusting tissue hardness, which is crucial for their defence against threats and adaptation to the environment.[1,2] For example, sea cucumbers can harden their bodies by triggering the crosslinking of collagen fibers to defend themselves against predators.[3–5] The leaves of the Venus flytrap change the mechanical stress within the cell walls by redistributing water between cells, enabling them to close and harden rapidly.[6–8] These examples provide abundant biomimetic inspiration for the construction of artificial materials with dynamically switchable stiffnesses. Inspired by this, polymer hydrogel materials synergistically integrate shape adaptability with load-bearing performance through on-demand modulation of their mechanical stiffness, thereby offering a promising approach for designing dynamic functional materials with broad application prospects.[9–24]

Currently, strategies for constructing polymer hydrogels with variable stiffness primarily include crystallization-melting phase transitions,[25–28] thermally induced phase separation,[17,28–31] supercooled crystallization,[32,33] ion coordination crosslinking,[34–36] and light-responsive dynamic bonding.[14,37] Through these approaches, hydrogels exhibit significant enhancements in their mechanical properties under various external stimuli. However, existing approaches generally rely on external energy inputs, including light, heat, electricity, or solvents, thereby increasing system complexity and inconvenience. For instance, crystallization-melting phase transitions require a continuous thermal energy supply, whereas light-responsive materials require specific wavelength light sources. Additionally, some systems require the introduction of additional chemicals (*e.g.*, utilizing supercooled ionic liquids for crystallization or inorganic ion coordination for enhanced crosslinking). These substances carry leakage risks during prolonged use and may reduce the repeatability of the stiffness regulation.

Water is one of the most abundant and environmentally friendly resources in nature and possesses unique advantages, such as mild conditions and low energy costs, making it an ideal stimulus source for regulating the stiffness of hydrogel materials.[38] However, traditional hydrogels typically exhibit poor mechanical properties in aqueous media be-

* Corresponding authors, E-mail: tao.chen@nimte.ac.cn (T.C.)
E-mail: luwei@nimte.ac.cn (W.L.)
Special Topic: Functional Gels
Received December 30, 2025; Accepted January 27, 2026; Published online April 17, 2026

cause of the plasticizing effect of water molecules and the weakened interactions between polymer chains, thus hindering their load-bearing applications in aquatic environments or high-humidity conditions.[39–42] In contrast, water-induced hardening of polymer hydrogels demonstrates enhanced stiffness upon contact with water. This anomalous water-mediated mechanical strengthening behavior significantly expands the flexibility and functionality of soft materials such as hydrogels in applications such as soft robots, bioelectronics, and artificial muscles.[43–49] Early studies on amphiphilic polymer networks have reported unusual poly(ethylene glycol) (PEG)-content-dependent mechanical responses upon hydration, showing rigidification when swelling of minority PEG-rich domains causes the majority of hyperbranched fluoropolymer (HBFP)-rich phases under stress, but pronounced softening when the majority PEG-rich phases were plasticized.[44] Recently, Zhu *et al*.[46] developed polymer gels by incorporating hydrophobic ionic liquids (IL) and hygroscopic lithium salts into a poly(benzyl methacrylate) network, which demonstrated a tens of thousand-fold increase in stiffness owing to water-driven phase separation. Wu *et al*.[47] reported an ionic gel composed of poly(*N*-isopropylacrylamide) and a hydrophobic IL that implemented dramatic water-induced stiffening through hydrogen-bonding competition-mediated phase separation. These polymer gels exhibited excellent water-induced mechanical enhancement properties. However, prolonged immersion in aqueous environments may cause leakage of the ionic liquids and inorganic salts used, leading to the direct failure of its stiffness regulation capability. This significantly limits the application potential of the water-induced stiffness enhancement of materials in more complex, programmable structures.

Herein, we propose and validate the utilization of polymers with hydrophilic/hydrophobic segments as a hydrogel matrix to enhance mechanical properties *via* water-induced phase separation (Scheme 1). Specifically, the poly[methyl methacrylate-*co*-poly(ethylene glycol) methacrylate] [P(MMA$_x$-*co*-OEGMA$_y$)] hydrogel was formed through the copolymerization of hydrophilic oligomeric glycidyl methacrylate (OEGMA) and hydrophobic methyl methacrylate (MMA). Upon contact with water, the hydrophilic OEGMA segments immediately formed strong hydrogen-bonded hydration layers with water molecules, driving the MMA segments to aggregate and form hydrophobic domains. This induced microscopic phase separation and constructed a physical cross-linking network, significantly enhancing the stiffness of the polymer hydrogel. Exposure of the reinforced polymer hydrogel to air caused a gradual loss of water, leading to the disassembly of the established phase-separated structure. The OEGMA and MMA segments reverted to their initial homogeneous structure, restoring the hydrogel to a soft state. Experiments demonstrated that this hydrogel can transition from a soft elastomer (1.88×10^{-2} MPa) to a high-strength material (201.63 MPa) solely upon water swelling, achieving a modulus enhancement of four orders of magnitude without significant volume or mass change. Notably, multistage stiffness enhancement can be effectively achieved by controlling the water-swelling duration. As a proof-of-concept, this hydrogel was employed for water-induced shape memory, and its application in multistage complex deformation programming with spatiotemporal coordinated regulation was explored.

EXPERIMENTAL

Materials

Methyl methacrylate (MMA≥99.5%) was provided by Sinopharm

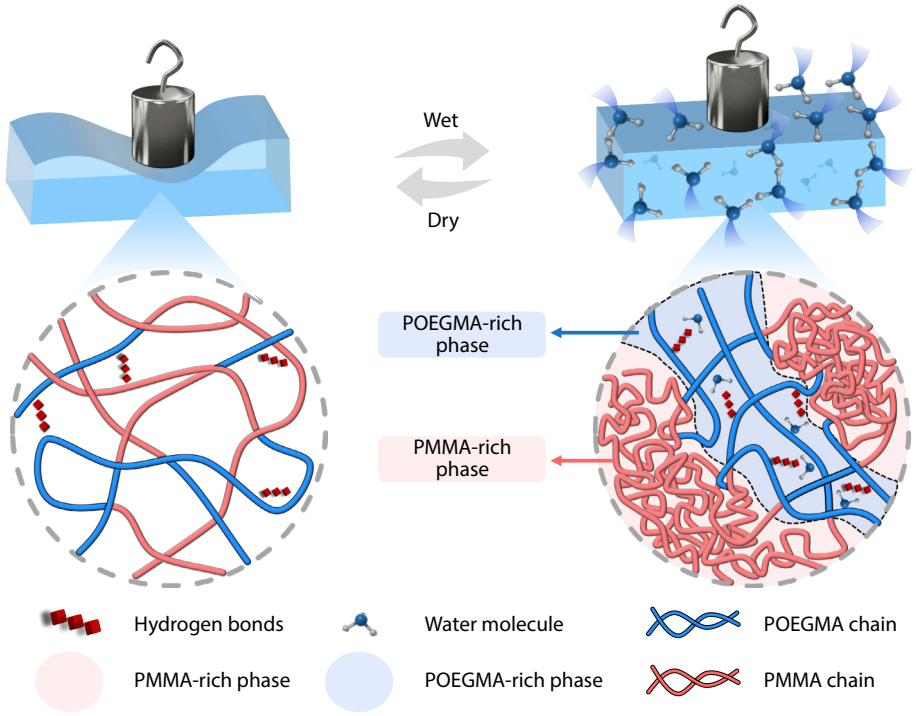

Scheme 1 Schematic illustration of water swelling-induced phase separation and stiffening of P(MMA$_x$-*co*-OEGMA$_y$) hydrogels.

https://doi.org/10.1007/s10118-026-3597-6

Chemical Reagent Co., Ltd. Poly(ethylene glycol) methacrylate (OEGMA, M_n is about 400) was purchased from Meryer Chemical Technology Co., Ltd. Purified 2,2'-Azobis(2-methylpropionitrile) (AIBN, 99%) was supplied by Shanghai Macklin Biochemical Co., Ltd. Ethylene glycol dimethacrylate (EGDMA) and dimethyl sulfoxide (DMSO) were purchased from Aladdin Industrial Co., Ltd. MMA and OEGMA were used after stabilizer removal. All other chemical reagents were used as received.

Preparation of the Poly[methyl methacrylate-*co*-poly(ethylene glycol) methacrylate] [P(MMA$_x$-*co*-OEGMA$_y$)] Hydrogel

Polymer hydrogels were prepared by random copolymerization of MMA and OEGMA with tunable monomer molar ratios, followed by a water-swelling process. The molar ratio of MMA to OEGMA was *x*:*y* for P(MMA$_x$-*co*-OEGMA$_y$). The AIBN content was fixed at 0.5 wt% relative to all monomers. For the typical P(MMA$_2$-*co*-OEGMA$_1$) copolymer film, 13.4 g of MMA (0.134 mol), 26.7 g of OEGMA (0.067 mol) and 0.2 g of AIBN (0.001 mol) were stirred at room temperature until thoroughly mixed. Subsequently, the mixed solution was injected into a custom-made glass mold with a 1- or 2-mm thick spacer. After radical polymerization in an oven at 60 °C for 10 h, a copolymer film was obtained. Other proportions of the copolymer films (P(MMA$_7$-*co*-OEGMA$_1$), P(MMA$_5$-*co*-OEGMA$_1$), and P(MMA$_3$-*co*-OEGMA$_1$)) were prepared using the same procedure by tuning the feed ratios. The as-prepared copolymer films were immersed in deionized water to yield the P(MMA$_x$-*co*-OEGMA$_y$) hydrogels.

Preparation of the P(MMA$_x$-*co*-OEGMA$_y$)-EGDMA Hydrogel

The preparation process for the P(MMA$_x$-*co*-OEGMA$_y$)-EGDMA hydrogel was similar to that described above. 6.7 g of MMA (0.0067 mol), 13.35 g of OEGMA (0.0335 mol), 0.1 g of AIBN (0.0005 mol) (0.1 g), and EGDMA (0.5 wt% of monomer mass) were mixed and stirred for 2 h at room temperature. The mixed solution was then poured into a custom-made glass mold (containing a 2 mm thick spacer), which was placed in an oven at 60 °C for 10 h to yield the copolymer film. Similarly, the as-prepared copolymer films were immersed in deionized water to obtain the P(MMA$_2$-*co*-OEGMA$_1$)-EGDMA hydrogels.

Characterization

^{1}H nuclear magnetic resonance (NMR)

^{1}H nuclear magnetic resonance (NMR) spectra of P(MMA$_x$-*co*-OEGMA$_y$) were tested by Bruker Advance AMX-400 spectrometer in $CDCl_3$.

Fourier-transform infrared (ATR-FTIR) test

Attenuated total reflectance Fourier-transform infrared (ATR-FTIR) spectroscopy was performed on a Thermo Fisher Scientific Nicolet FTIR spectrometer with 32 scans spanning the range of 4000–400 cm^{-1}.

Ultraviolet-visible (UV-Vis) test

Ultraviolet-visible (UV-Vis) transmittance spectra were recorded on a UV-Vis spectrophotometer (Lambda 1050+, Perkin Elmer Co., Ltd.), with all samples 1 mm thick.

Dynamic mechanical analysis (DMA) test

Dynamic mechanical analysis (DMA) was performed on a TA Q850 DMA instrument in shear and tensile modes to obtain the frequency sweep (strain = 0.1%) spectra at 25 °C.

Scanning electron microscope (SEM)

Scanning electron microscopy SEM (Hitachi S4800) was used to observe the microstructure of the hydrogels at an accelerating voltage of 4 kV and a current of 7 μA.

Mechanical property

Tensile tests were conducted using a Zwick universal test instrument (Zwick, Z1.0) with a 1000 N load cell at a tensile speed of 50 mm·min^{-1}. Dumbbell-shaped samples (35 mm × 6 mm × 1 mm) were used for the uniaxial tensile test. The ambient relative humidity during mechanical testing was maintained 20%–30%. The Young's modulus was calculated in the initial linear range from the stress-strain curve.

Small-angle X-ray scattering (SAXS) test

Small-angle X-ray scattering (SAXS) spectra were obtained using a 2D small-angle X-ray scattering instrument (Xeuss 3.0 UHR, XENOCS SAS, France) at a sample-detector distance of 1 m.

Volume-swelling ratio measurement

The as-prepared film samples were initially cut into squares measuring 1 cm × 1 cm and immersed in deionized water. The volume-swelling ratios (V_S) of the hydrogels were calculated using the following equation:

$$V_S = \frac{V_w}{V_0} \times 100\% \quad (1)$$

where V_w and V_0 represent the hydrogel volume at different water-swelling times and the as-prepared initial film volume, respectively.

Water content measurement

The as-prepared film samples were initially cut into squares measuring 1 cm × 1 cm and then weighed; the dry weight was recorded as W_{dry}. Subsequently, the film samples were immersed in deionized water, and the resulting wet weights at different water-swelling times were recorded as W_{wet}. The water content was calculated using the following equation:

$$W = \left(1 - \frac{W_{dry}}{W_{wet}}\right) \times 100\% \quad (2)$$

Evaluation of shape memory performance

The shape-memory behavior of the hydrogel was evaluated in an oven at 100 °C. The P(MMA$_2$-*co*-OEGMA$_1$) film strips (25 mm × 5 mm × 2 mm) were first manually bent at 90° and immersed in deionized water for different durations (1, 5, 10, 30, 60, and 120 min) to fix the temporary shape. The P(MMA$_2$-*co*-OEGMA$_1$) hydrogels were subsequently placed in an oven at 100 °C to record their recovery. The shape recovery ratio (R_r) was defined by the following equation:

$$R_r = \frac{\theta_r}{\theta_f} \times 100\% \quad (3)$$

where θ_r and θ_f represent the recovery angle and the hand-fixed shape angle, respectively.

RESULTS AND DISCUSSION

Fabrication and Optimization of P(MMA$_x$-*co*-OEGMA$_y$) Hydrogel

As depicted in Fig. 1(a) and Fig. S1 (in the electronic supplementary information, ESI), an amphiphilic copolymer film P(MMA$_x$-*co*-OEGMA$_y$) was synthesized *via* a one-step copolymerization method. The as-prepared films were based on hy-

drophobic methyl methacrylate (MMA) and hydrophilic oligomeric glycidyl methacrylate (OEGMA), where *x* and *y* denote the molar fractions of MMA and OEGMA in the copolymer, respectively. Given the distinct hydrophilic and hydrophobic nature of MMA and OEGMA, their molar ratios (*x*/*y*) within the copolymer would influence the initial mechanical properties of the as-prepared films. Therefore, a series of P(MMA_x-*co*-$OEGMA_y$) films with varying molar ratios was prepared using the same synthetic approach. As shown in Fig. S2 (in ESI), P(MMA_1-*co*-$OEGMA_1$) sample (*x*/*y*=1:1) did not form a mechanically stable film, suggesting that a sufficient MMA content (*x*≥2) was necessary for maintaining structural integrity. The absence of C=C bond absorption peaks in the region of 1640–1680 cm^{-1} in the Fourier-transform infrared (ATR-FTIR) spectra (Fig. S3 in ESI) and the region of 5.0–5.5 ppm in the ^1H nuclear magnetic resonance (NMR) spectra (Fig. S4 in ESI) confirmed the successful synthesis of all copolymer films. It could be observed that, in their initial state (prior to water swelling), all polymer films exhibited a highly transparent and homogeneous state (Fig. 1g and Fig. S5 in ESI). Notably, the P(MMA_2-*co*-$OEGMA_1$) film exhibited ultra-soft properties, sagging under its own weight when fixed at one end (Fig. 1g and Fig. S5 in ESI). As the proportion of hydrophilic OEGMA segments decreased, the films progressively became self-supporting and maintained a straight configuration. This phenomenon also paralleled the stress-strain curve and modulus variation trends observed in Figs. 1(b) and 1(c). The results suggested that both the tensile strength and Young's modulus exhibited a monotonic decreasing trend with increasing OEGMA content, whereas the elongation at break progressively increased. Remarkably, the P(MMA_7-*co*-$OEGMA_1$) film showed an initial modulus as high as 53.1 MPa, demonstrating typical rigid glassy behavior, whereas the P(MMA_2-*co*-$OEGMA_1$) film demonstrated a modulus of merely 0.0188 MPa. This substantial modulus contrast primarily arose from the extensive introduction of OEGMA segments, disrupting the close packing of the MMA segments. Consequently, the mobility of the polymer segment increased, manifesting macroscopically as a reduced modulus and enhanced flexibility. When all as-prepared films in the initial state were employed to lift weights, they could only withstand a 100 g load (Fig. 1g). Notably, the

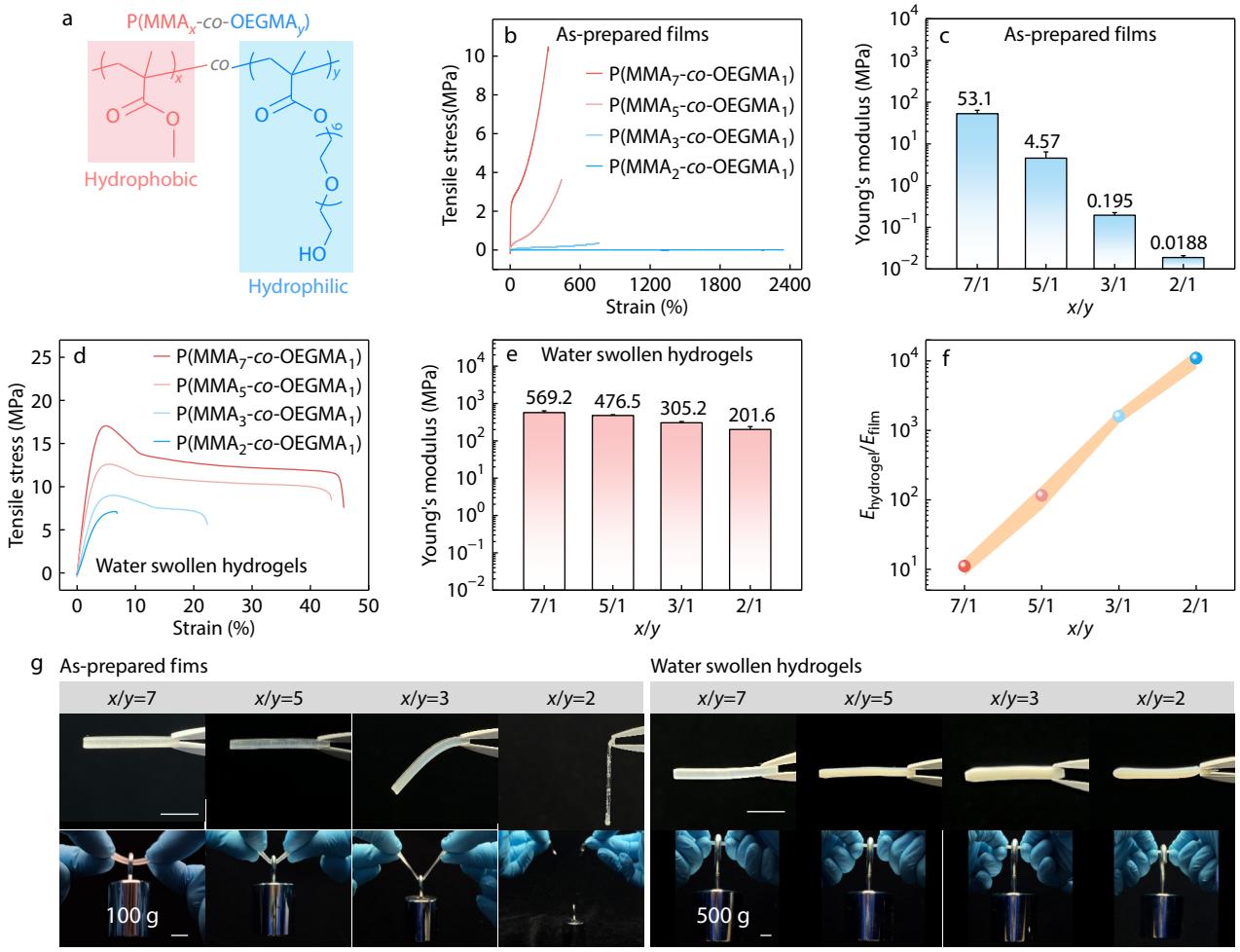

Fig. 1 Fabrication and optimization of P(MMA_x-*co*-$OEGMA_y$) hydrogels. (a) Schematic illustration of the chemical structure of P(MMA_x-*co*-$OEGMA_y$) hydrogels; (b) Stress-strain curves and (c) corresponding Young's modulus of as-prepared films (P(MMA_x-*co*-$OEGMA_y$)) with different molar ratios in the initial state; (d) Stress-strain curves and (e) corresponding Young's modulus of P(MMA_x-*co*-$OEGMA_y$) hydrogels with water swelling for 2 h; (f) Stiffness changes ($E_{hydrogel}/E_{film}$) of P(MMA_x-*co*-$OEGMA_y$) hydrogels; (g) Photographs demonstrating the mechanical properties of P(MMA_x-*co*-$OEGMA_y$) films/hydrogels in initial state and water swelling for 2 h, respectively. Scale bar is 1 cm.

https://doi.org/10.1007/s10118-026-3597-6

P(MMA$_2$-*co*-OEGMA$_1$) film fractured directly under a 100 g load owing to excessive softness.

After immersion in water for 2 h, all hydrogels transitioned from transparent to opaque and self-supported their weight in a horizontal state (Fig. 1g). Figs. 1(d) and 1(e) illustrate the stress-strain curves and modulus variations following 2 h of water swelling. All hydrogels displayed a dramatic water-swelling-induced mechanical strengthening effect, with significant increases in tensile strength and modulus, along with a marked reduction in fracture strain. Particularly, the modulus of P(MMA$_2$-*co*-OEGMA$_1$) hydrogel rose to 201.63 MPa after water swelling, showing an enhancement of four orders of magnitude compared to its initial state, with performance far surpassing that of previously reported amphiphilic copolymeric materials.[44,45] When water-swelling-induced strengthening occurred, all hydrogels could withstand a 500 g load without noticeable deformation (Fig. 1g). Quantitative analysis was conducted on the modulus enhancement factors of the hydrogels with different molar compositions. As depicted in Fig. 1(f), the modulus enhancement effect exhibited a positive correlation with the proportion of OEGMA, particularly where P(MMA$_2$-*co*-OEGMA$_1$) demonstrated the most pronounced water-swelling-induced strengthening behavior. Given that the P(MMA$_2$-*co*-OEGMA$_1$) hydrogel exhibited the broadest modulus modulation range, it was selected for the subsequent experiments.

The Transformation Process of Water Swelling-induced Stiffness Enhancement of Hydrogel

A systematic investigation into the influence of the water-swelling duration on the physical properties of the P(MMA$_2$-*co*-OEGMA$_1$) hydrogel. As shown in Fig. 2(a) and Movie S1 (in ESI), the hydrogel was highly transparent and homogeneous at the initial state (0 min). After immersion in water for 1 min, the film rapidly turned opaque and progressively whitened with increasing immersion time. When the immersion time was extended to 30 min, the hydrogel surface became completely opaque. With further extension of immersion time, the hydrogel remained stable. This phenomenon was speculated to arise mainly from water molecule-driven phase separation, wherein MMA aggregation formed hydrophobic domains that enhanced light scattering effects and consequently led to a reduction in transparency. Transmittance measurements (Fig. 2b) were used to quantify this change further. In the initial state, the hydrogel exhibited a transmittance as high as 90% in the range of 400–800 nm. After immersion for 1 min, the transmittance

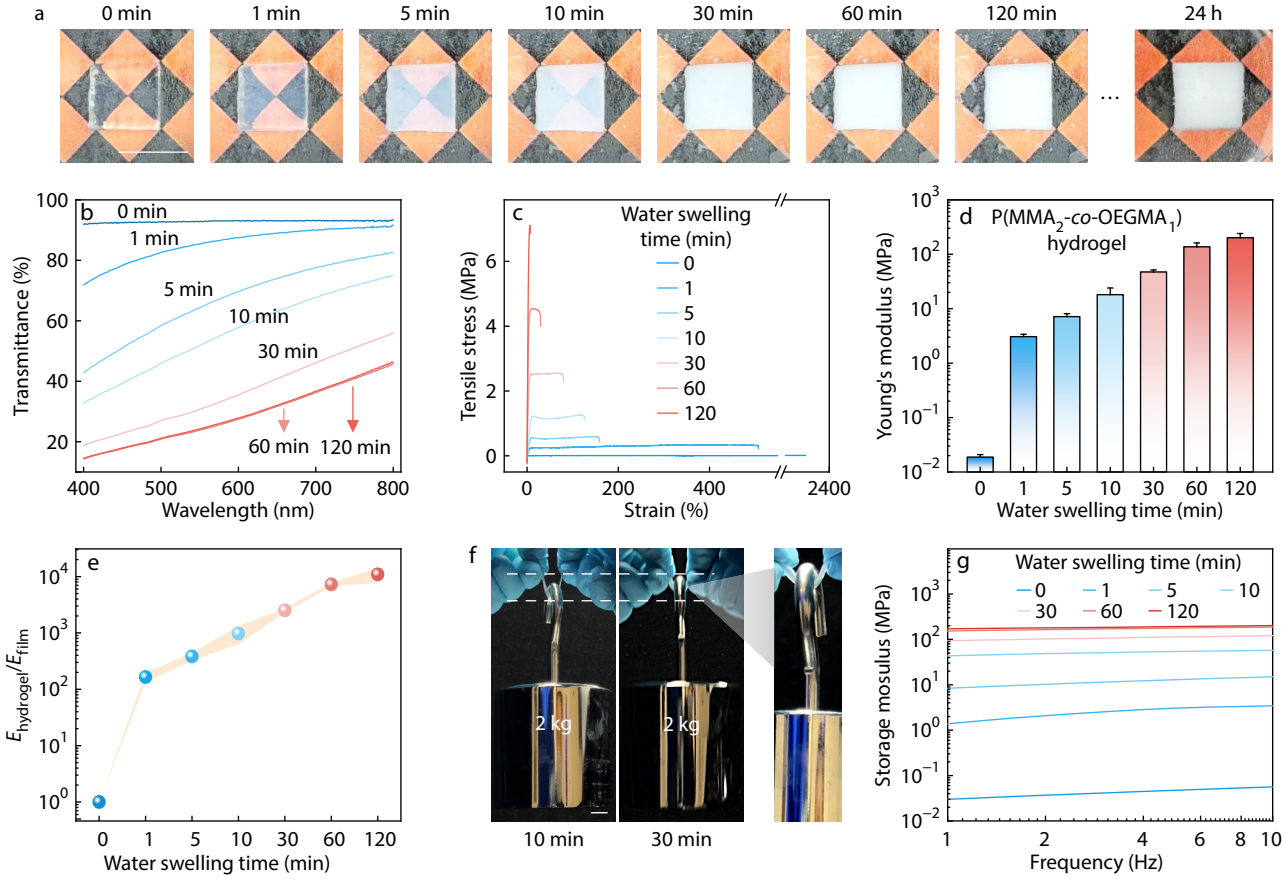

Fig. 2 The transformation process of water swelling-induced stiffness enhancement of P(MMA$_2$-*co*-OEGMA$_1$) hydrogel with water swelling. (a) Photos of the time-dependent transparency changes of P(MMA$_2$-*co*-OEGMA$_1$) hydrogel samples with water swelling. Scale bar is 1 cm. (b) The transmittance spectra, (c) stress-strain curves and (d) corresponding Young's modulus of P(MMA$_2$-*co*-OEGMA$_1$) hydrogel as a function of water swelling time. (e) Stiffness changes ($E_{hydrogel}/E_{film}$) of P(MMA$_2$-*co*-OEGMA$_1$) hydrogel; (f) Images of P(MMA$_2$-*co*-OEGMA$_1$) hydrogel with a holding up total 2 kg weights after 10 min and 30 min of water swelling. Scale bar is 1 cm. (g) Dynamic mechanical analysis as a function of water swelling time.

https://doi.org/10.1007/s10118-026-3597-6

decreased significantly and stabilized at a low stage at approximately 30 min, which was consistent with the trend of the macroscopic transparency variation. Even after continuous immersion for 24 h, the transmittance did not change, indicating that the phase-separated structure exhibited excellent stability. It is worth noting that no significant changes in the volume of the hydrogel were observed during the immersion process (Fig. S6 in ESI), thus avoiding internal high-stress issues in traditional hydrogels, which proved highly beneficial for practical applications.

This water-swelling time-dependent phase separation behavior also resulted in tunable macroscopic mechanical properties of the P(MMA_2-*co*-$OEGMA_1$) hydrogel. With an increase in the water-swelling time, both the tensile strength and Young's modulus exhibited an increasing trend, while the elongation at break gradually decreased (Figs. 2c–2e and Fig. S7 in ESI), indicating that the hydrogel gradually transformed from a soft elastomeric state to a rigid glassy state. For instance, the hydrogel immersed in water for 10 min could lift a 2 kg weight (Fig. 2f). After extending the water immersion time to 30 min, the same size hydrogel was able to sustain a 2 kg load while maintaining a smaller deformation, demonstrating that the prolonged water swelling time significantly enhanced the Young's modulus of the hydrogel. Figs. 2(d) and 2(e) show the quantitative relationships between the Young's modulus, modulus enhancement factor of the P(MMA_2-*co*-$OEGMA_1$) hydrogel, and water-swelling time. It was evident that the Young's modulus exhibited a trend of rapid increase, followed by stabilization with water swelling. After immersion for 1 min, the modulus increased rapidly from 1.88×10^{-2} MPa to approximately 50 MPa, representing a 2700-fold enhancement. Subsequently, the growth rate of the modulus slowed, showing a multi-stage increase behavior positively correlated with the water swelling duration. The water content changes during the process of water-swelling-induced stiffness enhancement of the P(MMA_2-*co*-$OEGMA_1$) hydrogel are shown in Fig. S8 (in ESI). This variation in stiffness enhancement stems from the synergistic effect of the water molecule penetration and phase separation. In the initial stage, water molecules diffused rapidly into the network, forming hydration layers with the OEGMA segments and driving the rapid aggregation of the hydrophobic MMA segments to form dense phases, leading to a sharp increase in the modulus. As the immersion time increased, hydration and phase separation gradually reached equilibrium, stabilizing the density of the dense phases and moderating modulus growth. To further clarify the role of solvent-polymer interactions, the P(MMA_2-*co*-$OEGMA_1$) film was immersed in dimethyl sulfoxide (DMSO). The P(MMA_2-*co*-$OEGMA_1$) film became completely softened and partially dissolved after approximately 50 min of immersion (Fig. S9 in ESI). This indicates that DMSO disrupted the aggregation of the hydrophobic MMA domain and hydrogen-bonding-mediated phase separation.

Dynamic mechanical analysis (DMA) further revealed the dynamic mechanical responses of the polymer gel (Fig. 2g and Fig. S10 in ESI). In the initial state, the storage modulus (G') of the hydrogel was low and exhibited a slight increase with increasing frequency, showing typical soft elastomer characteristics. After immersion for 1 min, G' increased significantly, indicating an enhanced hydrogel rigidity. As the water immersion time was further prolonged, the G' plateau displayed a stable variation within the frequency range of 1–10 Hz, demonstrating excellent dynamic mechanical stability. The G' curve after 60 min of immersion overlapped substantially with that at 120 min, further indicating that the mechanical properties reached a relatively stable state at approximately 60 min. This water-swelling-induced mechanical enhancement also improved the load-bearing capacity of the hydrogel under compressive loading. The P(MMA_2-*co*-$OEGMA_1$) hydrogel of the same size could easily support a weight of up to 5 kg without any deformation or fracture after 2 h of water swelling (Fig. S11 in ESI).

Mechanism of Water-induced Phase Separation

The scanning electron microscopy (SEM) images in Fig. 3(a) reveal the dynamic evolution of the internal microstructure of the P(MMA_2-*co*-$OEGMA_1$) hydrogel during the water-swelling-induced mechanical enhancement process. In the initial state (0 min), the cross-section of the hydrogel was smooth, indicating that the hydrophobic MMA and hydrophilic OEGMA segments formed a thermodynamically stable homogeneous network. After immersion in water for 1–5 min, sporadically distributed pores began to appear within the cross-section, indicating the initiation of the phase separation process. This occurred because water molecules rapidly permeated the network, disrupting the original homogeneous structures upon binding with the OEGMA hydrophilic segments and triggering the gradual aggregation of MMA hydrophobic segments. Small-angle X-ray scattering (SAXS) and its two-dimensional (2D) patterns were employed to monitor the microstructural changes in the P(MMA_2-*co*-$OEGMA_1$) hydrogel during the water-swelling-induced mechanical enhancement process.[50] As depicted in Fig. 3(b), compared to the initial state, both the slope and scattering intensity of the curve exhibited significant enhancement after 1 min of water swelling, indicating that water molecules rapidly combined with the hydrophilic OEGMA segments and induced the formation of hydrophobic MMA domains. As the water-swelling time increased, the scattering intensity gradually increased, suggesting an enhancement in the degree of phase separation. In the 2D SAXS patterns, a strengthened intensity of the scattering rings with prolonged water immersion could also be observed, confirming the increased aggregation and fusion of the polymer network and the formation of denser polymer phases (Fig. 3c).

Furthermore, ATR-FTIR spectra were employed to characterize the group interactions and structural evolution of the P(MMA_2-*co*-$OEGMA_1$) hydrogel before and after water immersion (Figs. 3d and 3e). First, a strong and broad O—H stretching vibration band emerged rapidly in the range of 3600–3200 cm^{-1}, indicating that water molecules quickly penetrated the polymer network and formed numerous hydrogen-bond interactions with the hydrophilic OEGMA segments. Notably, the O—H stretching vibration peak exhibited a gradual red shift from 3494 cm^{-1} to 3467 cm^{-1}, accompanied by an enhancement of the absorption intensity in the lower wavenumber region (3300–3200 cm^{-1}), suggesting the progressive formation of stronger hydrogen-bond networks, thereby constructing hydration layers.[51] Secondly, the ab-

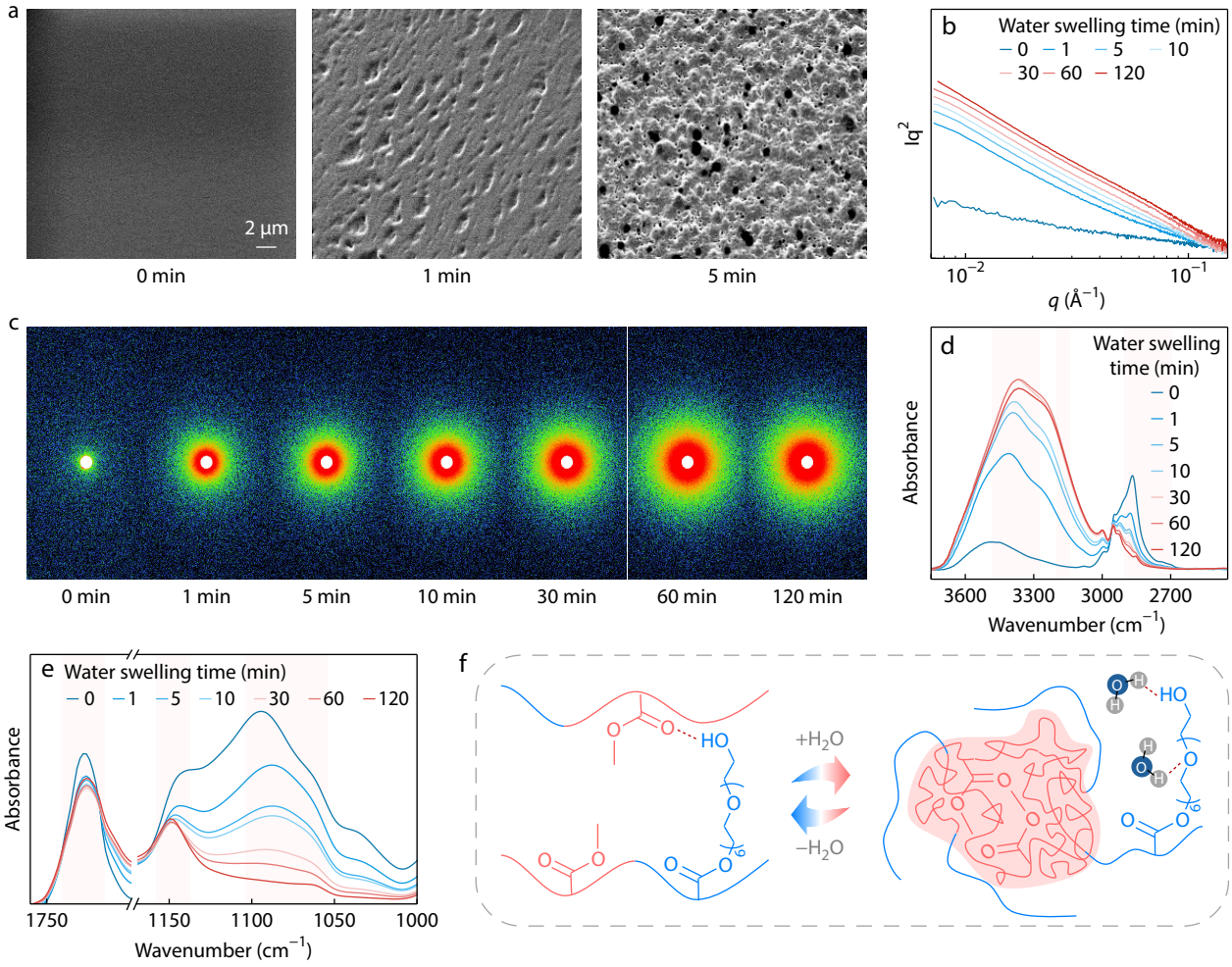

Fig. 3 Mechanism of water-induced phase separation of the P(MMA_2-*co*-$OEGMA_1$) hydrogel. (a) SEM images of the hydrogels after 0, 1 and 5 min of water swelling; (b) SAXS and (c) its two-dimensional (2D) patterns of P(MMA_2-*co*-$OEGMA_1$) hydrogels. (d, e) ATR-FTIR spectra of the hydrogels with different water swelling time: 0, 1, 5, 10, 30, 60 and 120 min; (f) Schematic diagram of the mechanism of water-induced hydrogen-bonding interactions and phase separation.

sorption peaks centered at 1727 and 1095 cm^{-1} exhibited distinct red shifts, corresponding to the carbonyl (C═O) and ether (C—O—C) groups, respectively.[52,53] These spectral changes indicate that dynamic hydrogen-bonding interactions formed between water molecules and the carbonyl and ether groups upon hydration. Additionally, the vibration band near 1150 cm^{-1} gradually shifted toward higher wavenumbers with prolonged water immersion, which can be attributed to the densification and aggregation of hydrophobic MMA-enriched domains induced by hydration-driven segmental rearrangement.[54] Consistently, stretching vibration peaks of —CH_2 and —CH_3 (3000–2800 cm^{-1}) exhibited a blue shift with prolonged immersion time, corresponding to hydration-induced densification of the OEGMA region and enhanced aggregation of the hydrophobic MMA domain[55]. These spectral changes collectively revealed that the polymer-polymer interactions were gradually disrupted, ultimately leading to phase separation (Fig. 3f).

To validate the role of chain mobility in water-swelling-induced stiffness enhancement, we prepared a control sample containing the covalent crosslinker ethylene glycol dimethacrylate (EGDMA): P(MMA_2-*co*-$OEGMA_1$)-EGDMA hydrogel. As shown in Fig. S12 (in ESI), in the initial state, the crosslinked P(MMA_2-*co*-$OEGMA_1$)-EGDMA film was fully transparent and could readily support a load of 100 g, indicating a higher initial stiffness than that of the non-crosslinked P(MMA_2-*co*-$OEGMA_1$) film. After immersion in water for 2 h, the crosslinked P(MMA_2-*co*-$OEGMA_1$)-EGDMA hydrogel remained transparent, suggesting that there was no pronounced water swelling-induced phase separation. Under a higher load of 500 g, the crosslinked hydrogel exhibited noticeable deformation, indicating that the effect of the water-swelling-induced stiffness enhancement was far inferior to that of the non-crosslinked P(MMA_2-*co*-$OEGMA_1$) hydrogel. These results indicate that the high mobility of the segments in this system, unlike that of chemically cross-linked amphiphilic polymer networks, enabled hydration-driven segmental rearrangement and phase separation.[44]

Shape Memory Property

Based on the exceptional water-swelling-induced stiffening performance of the P(MMA_2-*co*-$OEGMA_1$) hydrogel, its application in shape memory and time-dependent reversible shape pro-

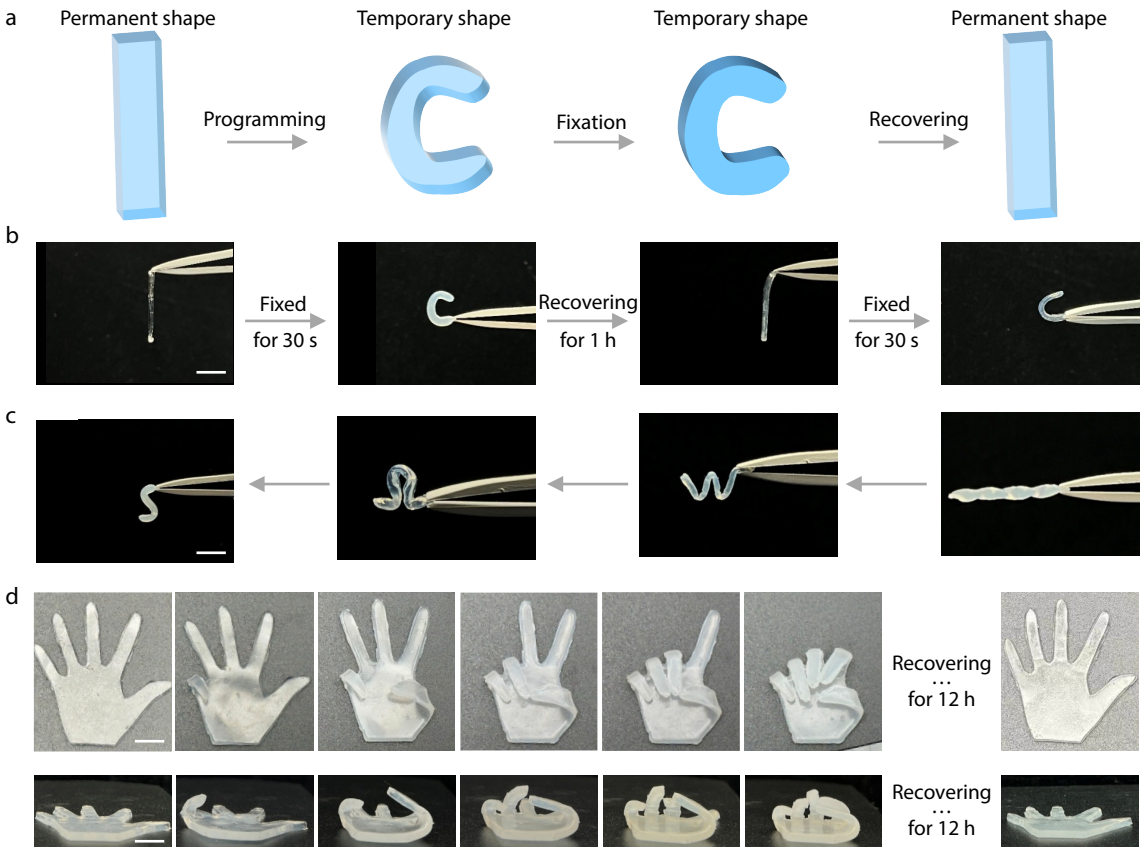

Fig. 4 Demonstration of P(MMA$_2$-*co*-OEGMA$_1$) hydrogel as water-induced shape memory materials. (a) Schematic diagram of the shape memory process; (b) Photos exhibiting water-induced shape memory cycle of the P(MMA$_2$-*co*-OEGMA$_1$) hydrogel; (c) Photos of various shape memory information; (d) Top view and front view of shape programming and recovery of the hand-shaped hydrogel. Scale bar is 1 cm.

gramming was explored (Fig. 4a). For quantitative analysis, the shape-memory performance of the P(MMA$_2$-*co*-OEGMA$_1$) hydrogel was evaluated. The P(MMA$_2$-*co*-OEGMA$_1$) films were manually bent at 90° and immersed in deionized water for different durations (1, 5, 10, 30, 60, and 120 min) to fix the temporary shape. After water swelling, the P(MMA$_2$-*co*-OEGMA$_1$) hydrogels were fixed vertically using a clamp and their recovery processes were monitored in an oven at 100 ℃. As shown in Fig. S13 (in ESI), the recovery time increased with prolonged water immersion, indicating a strong dependence of the recovery kinetics on the water swelling time. Notably, the samples immersed less than 30 min could recover to 100% within 10 min at 100 ℃, while the samples soaked for 60 and 120 min exhibited superior shape fixation capabilities. This indicates that prolonged water swelling induced strong hydration-driven phase separation, impeding shape recovery. As shown in Fig. 4(b), in the initial state, the strip-shaped polymer hydrogel could not support its own weight owing to its low modulus, and thus, exhibited a natural drooping state. The hydrogel was manually programmed into a "C" shape and simultaneously immersed in water for 30 s to achieve rapid modulus enhancement, which locked the deformed temporary shape. After the hydrogel was left resting in the air (relative humidity 20%–30%) for 1 h, with the gradual evaporation of water, the modulus decreased, and the hydrogel spontaneously recovered to its initial drooping morphology as it softened. Owing to the reversibility of the water absorption and water evaporation processes, the same initially drooping gel could be easily programmed into various temporary shapes such as spiral, "Ω," "W," and twist knot, demonstrating excellent reversibility of multi-shape programming (Fig. 4c). Finally, the P(MMA$_2$-*co*-OEGMA$_1$) hydrogel was patterned into a human hand shape and multistage shape programming under spatiotemporal synergistic control was explored. As shown in Figs. 4(d) and 4(e), the expanded palm could be manipulated through stepwise bending of fingers followed by water-induced fixation, allowing various temporary gestures such as the "V" gesture and single-finger bending to be achieved. After being exposed to air for 12 h, the water evaporated, leading to a decrease in the modulus, and all fingers spontaneously recovered to their initial unfolded state. A similar water-triggered spatiotemporal regulation of shape programming was further confirmed for the reversible transformation between the 2D and 3D windmill patterns (Fig. S14 in ESI). The spatiotemporally dependent, water-induced dynamic modulus switching behavior of the P(MMA$_2$-*co*-OEGMA$_1$) hydrogel provides a foundation for the controllable programming of multistage complex shapes.

CONCLUSIONS

In summary, we proposed a promising water-swelling-induced phase separation strategy for developing water-stimuli-responsive hydrogel systems with dynamically tunable stiffness. The material was formed *via* one-step polymerization of hydrophilic

oligomeric glycidyl methacrylate (OEGMA) and hydrophobic methyl methacrylate (MMA). Upon water stimulation, strong hydrogen-bonding interactions are formed between the hydrophilic OEGMA groups and water molecules, which drive the aggregation of the hydrophobic MMA segments. This process forms numerous dense hydrophobic domains that act as dynamic physical cross-linking sites, thereby enhancing the macroscopic mechanical properties of hydrogels. Triggered by water, the modulus of the hydrogel can increase from 0.0188 MPa to 201.6 MPa, enabling reversible switching between elastomer-like and glass-like states. Notably, precise regulation of the hydrogel modulus can be achieved by controlling the duration of water swelling and realizing multi-stage stiffness modulation. Furthermore, the hydrogel exhibited water-induced shape memory behavior, enabling temporary shape fixation for the controllable programming of multistage complex shapes. This water-swelling-induced stiffness enhancement strategy offers novel insights for developing high-performance smart gel materials, advancing their practical applications in soft robotics and biomedical devices.

Conflict of Interests

The authors declare no interest conflict.

Electronic Supplementary Information

Electronic supplementary information (ESI) is available free of charge in the online version of this article at http://doi.org/10.1007/s10118-026-3597-6.

Data Availability Statement

The data supporting the findings of this study are available from the corresponding author upon reasonable request.

ACKNOWLEDGMENTS

This work was financially supported by the National Natural Science Foundation of China (Nos. 52473116 and 22322508), Zhejiang Provincial Natural Science Foundation of China (Nos. LR23E030001 and LD26E030001), and Natural Science Foundation of Ningbo (No. 2024S069).

REFERENCES

1 Ganewatta, M. S.; Wang, Z.; Tang, C. Chemical syntheses of bioinspired and biomimetic polymers toward biobased materials. *Nat. Rev. Chem.* **2021**, *5*, 753–772.
2 Shanmuganathan, K.; Capadona, J. R.; Rowan, S. J.; Weder, C. Biomimetic mechanically adaptive nanocomposites. *Prog. Polym. Sci.* **2010**, *35*, 212–222.
3 Thurmond, F. A.; Trotter, J. A. Morphology and biomechanics of the microfibrillar network of sea cucumber dermis. *J. Exp. Biol.* **1996**, *199*, 1817–1828.
4 Szulgit, G. K.; Shadwick, R. E. Dynamic mechanical characterization of a mutable collagenous tissue: response of sea cucumber dermis to cell lysis and dermal extracts. *J. Exp. Biol.* **2000**, *203*, 1539–1550.
5 Mo, J.; Prévost, S. F.; Blowes, L. M.; Egertová, M.; Terrill, N. J.; Wang, W.; Elphick, M. R.; Gupta, H. S. Interfibrillar stiffening of echinoderm mutable collagenous tissue demonstrated at the nanoscale. *Proc. Natl. Acad. Sci.* **2016**, *113*, E6362–E6371.
6 Hodick, D.; Sievers, A. On the mechanism of trap closure of venus flytrap (dionaea muscipula ellis). *Planta* **1989**, *179*, 32–42.
7 Forterre, Y.; Skotheim, J. M.; Dumais, J.; Mahadevan, L. How the venus flytrap snaps. *Nature* **2005**, *433*, 421–425.
8 Volkov, A. G.; Adesina, T.; Markin, V. S.; Jovanov, E. Kinetics and mechanism of dionaea muscipula trap closing. *Plant Physiology* **2008**, *146*, 323–324.
9 Duan, J.; Zhang, L. Robust and smart hydrogels based on natural polymers. *Chinese J. Polym. Sci.* **2017**, *35*, 1165–1180.
10 Wu, J. J.; Huang, L. M.; Zhao, Q.; Xie, T. 4D printing: history and recent progress. *Chinese J. Polym. Sci*. **2018**, *36*, 563–575.
11 Bao, B.; Zeng, Q.; Li, K.; Wen, J.; Zhang, Y.; Zheng, Y.; Zhou, R.; Shi, C.; Chen, T.; Xiao, C.; Chen, B.; Wang, T.; Yu, K.; Sun, Y.; Lin, Q.; He, Y.; Tu, S.; Zhu, L. Rapid fabrication of physically robust hydrogels. *Nat. Mater.* **2023**, *22*, 1253–1260.
12 Ishikawa, S.; Iwanaga, Y.; Uneyama, T.; Li, X.; Hojo, H.; Fujinaga, I.; Katashima, T.; Saito, T.; Okada, Y.; Chung, U.; Sakumichi, N.; Sakai, T. Percolation-induced gel-gel phase separation in a dilute polymer network. *Nat. Mater.* **2023**, *22*, 1564–1570.
13 Lin, X.; Wang, X.; Cui, H.; Rao, P.; Meng, Y.; Ouyang, G.; Guo, H. Hydrogels with ultra-highly additive adjustable toughness under quasi-isochoric conditions. *Mater. Horiz.* **2023**, *10*, 993–1004.
14 Liu, C.; He, C.; Dai, X.; Yan, L.; Xu, H. Achieving mechanical evolution in polymer materials through phase evolution induced by visible light. *Adv. Mater*. **2025**, e08549.
15 Chen, L.; Yin, Y.; Liu, Y.; Lin, L.; Liu, M. Design and fabrication of functional hydrogels through interfacial engineering. *Chinese J. Polym. Sci.* **2017**, *35*, 1181–1193.
16 Zhang, Y.; Zhao, W.; Ma, S.; Liu, H.; Wang, X.; Zhao, X.; Yu, B.; Cai, M.; Zhou, F. Modulus adaptive lubricating prototype inspired by instant muscle hardening mechanism of catfish skin. *Nat. Commun.* **2022**, *13*, 377.
17 Wu, J.; Wu, B.; Xiong, J.; Sun, S.; Wu, P. Entropy-mediated polymer-cluster interactions enable dramatic thermal stiffening hydrogels for mechanoadaptive smart fabrics. *Angew. Chem. Int. Ed.* **2022**, *61*, e202204960.
18 Liu, D.; Jiang, P.; Wang, Y.; Lu, Y.; Wu, J.; Xu, X.; Ji, Z.; Sun, C.; Wang, X.; Liu, W. Engineering tridimensional hydrogel tissue and organ phantoms with tunable springiness. *Adv. Funct. Mater.* **2023**, *33*, 2214885.
19 Han, Y. Q.; Lei, Z. Y.; Wu, P.Y. Mxene nanosheet-enhanced ionotronic hydrogels for wireless powering and noncontact sensing. *Chinese J. Polym. Sci.* **2025**, *43*, 572–580.
20 Chen, D.; Wang, H. J.; Ni, C. J.; Chen, J. Y.; Guo, Y. J.; Chen, Z.; Zheng, N.; Wu, J. J.; Ren, H.; Zhao, Q. Light-regulated microstructure growth of dynamic hydrogels for flexible manufacturing of microlens arrays. *Chem Bio Eng.* **2025**, *2*, 350–357.
21 Li, J. S.; Hu, Z. Q.; Zhang, H. W.; Ji, X. F. Poly[2]catenanes-based hydrogels prepared by hydroxyl-yne click chemistry. *Supramolecular Materials* **2024**, *3*, 100076.
22 Qiu, J. X.; Ma, H. D.; Yao, M. T.; Song, M. T.; Zhang, L. P.; Xu, J. K.; Liu, X. M.; Lu, B. Y. Design of a supersoft, ultra-stretchable, and 3d printable hydrogel electrical bioadhesive interface for electromyography monitoring. *Supramolecular Materials* **2024**, *3*, 100079.
23 Lu, W.; Si, M. Q.; Le, X. X.; Chen, T. Mimicking color-changing organisms to enable the multicolors and multifunctions of smart fluorescent polymeric hydrogels. *Acc. Chem. Res.* **2022**, *55*, 2291–2303.

Graphical Abstract

Water Swelling-induced Stiffness Enhancement of Polymer Hydrogels

Yi Yu, Wei Zhou, Tao Chen, and Wei Lu

Ningbo Institute of Materials Technology and Engineering, Chinese Academy of Sciences; University of Chinese Academy of Sciences

A hydrogel film based on the synergistic interaction of hydrophilic and hydrophobic side chains was successfully developed and achieved reversible stiffness changes spanning four orders of magnitude *via* the formation and dissociation of water-induced phase separation.

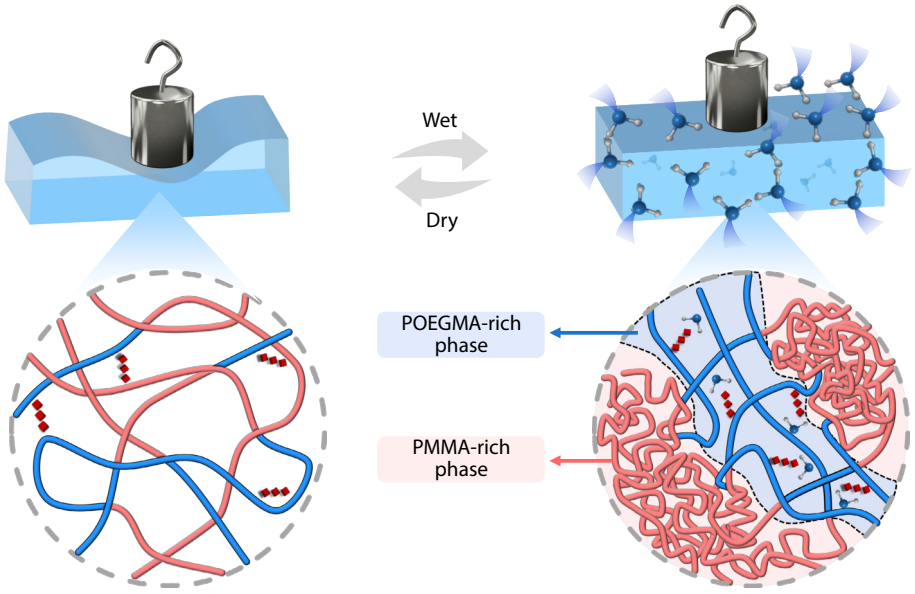

Chinese J. Polym. Sci., 2026 *https://doi.org/10.1007/s10118-026-3597-6*

24 Feng, W. H.; Li, F.; Jiang, Z. Y.; Yue, C. J.; Yin, G. Q.; Zhu, N.; Zhang, K.; Chen, T.; Lu, W. Supramolecular entanglement driven emissive aggregate densification enabling room-temperature phosphorescence hydrogels with ultrastretchability and crack-tolerance. *Angew. Chem. Int. Ed.* **2025**, *64*, e202505192.

25 Zhou, Y.; Yu, C.; Zhang, X.; Zheng, Y.; Wang, B.; Bao, Y.; Shan, G.; Wang, H.; Pan, P. Ultrasensitive ionic conductors with tunable resistance switching temperature enabled by phase transformation of polymer cocrystals. *Adv. Mater.* **2024**, *36*, 2309568.

26 Zhao, X.; Peng, L. M.; Chen, Y.; Zha, X. J.; Li, W. D.; Bai, L.; Ke, K.; Bao, R. Y.; Yang, M. B.; Yang, W. Phase change mediated mechanically transformative dynamic gel for intelligent control of versatile devices. *Mater. Horiz.* **2021**, *8*, 1230−1241.

27 Zhou, W.; Han, Y.; Xiao, P.; Yu, Y.; Wang, Y. C.; Chen, T. Interfacial elastic film with temperature mediated-phase transition behavior for tunable suspended sensing. *Chinese J. Polym. Sci.* **2025**, *43*, 1155−1162.

28 Nonoyama, T.; Lee, Y. W.; Ota, K.; Fujioka, K.; Hong, W.; Gong, J. P. Instant thermal switching from soft hydrogel to rigid plastics inspired by thermophile proteins. *Adv. Mater.* **2020**, *32*, 1905878.

29 Zhao, Y.; Wu, B.; Sun, S.; Wu, P. Chemical fuel-driven stiffening of transient hydrogels *via* vitrifiable phase separation. *Angew. Chem. Int. Ed.* **2025**, *64*, e202518064.

30 Li, H. B.; Bian, Q. Y. Stimuli-responsive protein hydrogels: from dynamic tuning of hydrogel mechanics to shape morphing. *Supramolecular Materials.* **2025**, *4*, 100120.

31 Wei, M.; Han, J. Y.; Yu, C.; Li, P.; Zhang, X. Y.; Ding, J. H.; Chen, M. W.; Li, X. K.; Yin, G. Q.; Zhang, T.; Wang, J. G.; Théato, P; Chen, T.; Lu, Wei. Mass diffusion-dominated phase separation enabling on-demand and repeatable lifetime programming of room-temperature phosphorescence polymer hydrogels. *Adv. Mater.* **2025**, e17109.

32 Ming, X.; Zhang, D.; Zhu, H.; Zhang, Q.; Zhu, S. Tremendous stiffness-changing polymer networks enabled by touch-induced crystallization. *Adv. Funct. Mater.* **2024**, *34*, 2411560.

33 Wang, S.; Liu, H.; Yu, Z.; Ren, X.; Hua, Q.; Panahi-Sarmad, M.; Yang, P.; Liu, C.; Renneckar, S.; Liu, H.; Jiang, F. Cellulose-mediated ionic liquid crystallization enables tough-stiff switchable ionogels. *Nat. Commun.* **2025**, *16*, 9007.

34 Lee, J.; Castilho, R. M.; Nam, S. Spatiotemporal toughness modulation in hydrogels through on-demand cross-linking. *Sci. Adv.* **2025**, *11*, eadz0440.

35 Hou, R.; Xu, L. J.; Yu, M. L.; Tang, Z. M.; Zhou, B.; Zhang, Q.; Li, N.; Xu, J. X. Piezoelectric-triboelectric hybrid nanogenerator based on tough, stretchable batio$_3$ doped antibacterial hydrogel for self-powered sensors. *Supramolecular Materials* **2025**, *4*, 100096.

36 Yan, D. D.; Zhu, S. L.; Zhao, H. Y.; Feng, S. H; Kang, B. B.; Yang, X.;

Zhang, Y. J.; Li, Z. Z.; Yu, W. W.; Ye, Y. N. Organic-inorganic nanocomposite organogel with double-network topology for enhanced mechanical and dielectric properties. *Supramolecular Materials* **2025**, *4*, 100112.
37 Wu, Z.; Kong, H.; Wang, J.; Guan, J.; Yin, M. Photo-responsive peptide hydrogels with tunable stiffness *via* water switching for cell fate regulation. *Adv. Funct. Mater*. **2025**, e26641.
38 Ma, M.; Guo, L.; Anderson, D. G.; Langer, R. Bio-inspired polymer composite actuator and generator driven by water gradients. *Science* **2013**, *339*, 186–189.
39 Itagaki, H.; Kurokawa, T.; Furukawa, H.; Nakajima, T.; Katsumoto, Y.; Gong, J. P. Water-induced brittle-ductile transition of double network hydrogels. *Macromolecules* **2010**, *43*, 9495–9500.
40 Gong, K.; Hou, L.; Wu, P. Hydrogen-bonding affords sustainable plastics with ultrahigh robustness and water-assisted arbitrarily shape engineering. *Adv. Mater.* **2022**, *34*, 2201065.
41 Xu, Z.; Wu, M.; Gao, W.; Bai, H. A sustainable single-component "silk nacre." *Sci. Adv*. **2022**, *8*, eabo0946.
42 Yang, C.; Zheng, W. Z.; Ni, C. J.; Li, Y.;Chen, D.; Xie, T.; Zhao, Q. Reconfigurable and orthogonal stiffness-structure patterning of dynamically crosslinked amphigels. *SmartMat.* **2024**, *5*, e1255.
43 Wang, Z.; Qiu, W.; Zhang, Q. Constructing phase separation in polymer gels: strategies, functions and applications. *Prog. Polym. Sci.* **2024**, *154*, 101847.
44 Xu, J.; Bohnsack, D. A.; Mackay, M. E.; Wooley, K. L. Unusual mechanical performance of amphiphilic crosslinked polymer networks. *J. Am. Chem. Soc.* **2007**, *129*, 506–507.
45 Bedoui, F.; Widjaja, L. K.; Luk, A.; Bolikal, D.; Murthy, N. S.; Kohn, J. Anomalous increase in modulus upon hydration in random copolymers with hydrophobic segments and hydrophilic blocks. *Soft Matter* **2012**, *8*, 2230.
46 Ming, X.; Yao, L.; Zhu, H.; Zhang, Q.; Zhu, S. Dramatic and reversible water-induced stiffening driven by phase separation within polymer gels. *Adv. Funct. Mater.* **2022**, *32*, 2109850.
47 Xu, J.; Wu, B.; Hou, L.; Wu, P. Hydrogen bonding competition mediated phase separation with abnormal moisture-induced stiffness boosting. *Small* **2024**, *20*, 2401164.
48 Li, M.; Lu, H.; Pi, M.; Zhou, H.; Wang, Y.; Yan, B.; Cui, W.; Ran, R. Water-induced phase separation for anti-swelling hydrogel adhesives in underwater soft electronics. *Adv. Sci.* **2023**, *10*, 2304780.
49 Yu, K.; Feng, Z.; Du, H.; Lee, K. H.; Li, K.; Zhang, Y.; Masri, S. F.; Wang, Q. Constructive adaptation of 3d-printable polymers in response to typically destructive aquatic environments. *PNAS Nexus* **2022**, *1*, pgac139.
50 Shibayama, M. Small-angle neutron scattering on polymer gels: phase behavior, inhomogeneities and deformation mechanisms. *Polym. J.* **2011**, *43*, 18–34.
51 Ikemoto, Y.; Harada, Y.; Tanaka, M.; Nishimura, S.; Murakami, D.; Kurahashi, N.; Moriwaki, T.; Yamazoe, K.; Washizu, H.; Ishii, Y.; Torii, H. Infrared spectra and hydrogen-bond configurations of water molecules at the interface of water-insoluble polymers under humidified conditions. *J. Phys. Chem. B* **2022**, *126*, 4143–4151.
52 Yao, X.; Dunn, S. S.; Kim, P.; Duffy, M.; Alvarenga, J.; Aizenberg, J. Fluorogel elastomers with tunable transparency, elasticity, shape-memory, and antifouling properties. *Angew. Chem. Int. Ed.* **2014**, *53*, 4418–4422.
53 Ren, Y.; Liu, Z.; Jin, G.; Yang, M.; Shao, Y.; Li, W.; Wu, Y.; Liu, L.; Yan, F. Electric-field-induced gradient ionogels for highly sensitive, broad-range-response, and freeze/heat-resistant ionic fingers. *Adv. Mater.* **2021**, *33*, 2008486.
54 Li, M.; Chen, L.; Li, Y.; Dai, X.; Jin, Z.; Zhang, Y.; Feng, W.; Yan, L.-T.; Cao, Y.; Wang, C. Superstretchable, yet stiff, fatigue-resistant ligament-like elastomers. *Nat. Commun.* **2022**, *13*, 2279.
55 Sel, E.; Ulu, A.; Ateş, B.; Köytepe, S. Comparative study of catalase immobilization *via* adsorption on p(mma-co-peg500ma) structures as an effective polymer support. *Polym. Bull.* **2021**, *78*, 2663–2684.

https://doi.org/10.1007/s10118-026-3597-6